Modeling and Design of EMI Noise Separators for Multiphase Power Electronics Systems

Shuo Wang, *Senior Member, IEEE*

***Abstract*—This paper first discusses the electromagnetic interference (EMI) noise in multiphase power electronics systems using symmetrical component theory and EMI theory. The theory for multiphase noise separators is developed. Multiphase noise separators are characterized by S-parameters based on symmetrical component theory, S-parameter theory, and EMI theory. A circuit is proposed for multiphase noise separators and techniques are explored for a high-quality design. A prototype is built, tested, and evaluated using the developed theory. The prototype is finally used in a practical EMI measurement.**

***Index Terms*—Common-mode transmission ratio (CMTR), common-mode rejection ratio (CMRR), differential-mode rejection ratio (DMRR), differential-mode transmission ratio (DMTR), electromagnetic interference (EMI), multiphase, noise separator, scattering parameters, symmetrical-component theory, three-phase, transmission line transformer.**

I. Introduction

THE conducted electromagnetic interference (EMI) is a headache problem for the design of power electronics systems. In high-power applications, such as three-phase or multiphase power electronics systems, due to high *dv/dt*, the large parasitic capacitance between high *dv/dt* nodes and the ground, and high-current ripples, EMI noise is much higher than the noise limits defined in EMI standards such as MIL-STD-461 and DO-160. To suppress EMI so as to meet the EMI standards, huge EMI filters are needed. On the other hand, high power density is one of the most important aspects used to evaluate a power electronics system in modern power electronics industry. The power density of a power electronics system is defined as the output power over the volume of the system, so the power density would be reduced if the EMI filter is big. In some applications, such as motor drive systems, the power density of the power electronics systems can be reduced by 50% due to the volume increased by EMI filters [1]. The EMI filter design should be optimized to minimize EMI filter's size. Conventionally, conducted EMI is divided into two categories: differential mode (DM) noise and common mode (CM) noise. DM noise flows within lines and CM noise flows between the lines and the ground. The EMI filter must suppress both DM and CM noises. Unfortunately, the conducted EMI standards for power electronics applications do not differentiate DM and CM noises; only the noise measured on line impedance stabilization networks (LISNs) is defined in the standards. The noise measured on LISN is either the sum or difference of DM and CM noises, so they are not separated. Engineers cannot make an efficient DM and CM filter design based on the noise directly measured on LISNs.

Noise separators were introduced to separate DM and CM noises in papers [2], [9]–[18]. Most of the publications address two-phase noise separators only. This paper will address multiphase noise separators using S-parameter theory, symmetrical component theory, and EMI theory. This paper will propose a modeling technique to characterize and evaluate multiphase noise separators. The circuit structure for multiphase noise separators is proposed. The prototype is built, evaluated, and tested. The proposed noise separator can help engineers to optimize the EMI filter design so as to greatly improve systems' power density. This paper actually generalizes the modeling and design techniques for noise separators, so that they can be applied to any *n*-phase power electronics systems, including single-phase and three-phase power electronics systems. The developed device can also be used to measure the unbalance of multiphase networks and devices [20], so it is a very useful device.

This paper will first describe a typical three-phase EMI measurement setup. DM and CM noises are defined for three-phase and multiphase systems based on symmetrical component theory. The functions of the noise separator are identified and its critical parameters are defined. The multiphase noise separator is modeled using S-parameter theory. The critical parameters of the noise separator are characterized using S-parameters and signal-flow graph. The circuit structure for a noise separator is proposed to achieve multiphase noise separations. The noise separator design is investigated and improved with the help of multiconductor transmission line theory. A noise separator prototype is finally built, evaluated, and used in a practical three-phase power electronics system for EMI measurement and diagnosis.

II. DM and CM Noises in Multiphase Power Electronics Systems

A typical EMI noise measurement setup for a three-phase power electronics system is shown in Fig. 1. Parasitic capacitance, especially the parasitic capacitance $C_{\rm CM}$ between the high *dv/dt* nodes and the ground, offers paths for CM noise. The CM noise $3\mathbf{I}_{\mathbf{CM}}$ comes back to the system through 50 Ω terminations and LISNs. DM noises $\mathbf{I}_{\mathbf{DM1}}$, $\mathbf{I}_{\mathbf{DM2}}$, and

Manuscript received November 3, 2010; revised January 15, 2011; accepted March 11, 2011. Date of current version November 18, 2011. Recommended for publication by Associate Editor J.-L. Schanen.

The author is with the Department of Electrical and Computer Engineering, University of Texas at San Antonio, San Antonio, TX 78249 USA (e-mail: shuowang@ieee.org).

Color versions of one or more of the figures in this paper are available online at http://ieeexplore.ieee.org.

Digital Object Identifier 10.1109/TPEL.2011.2136440

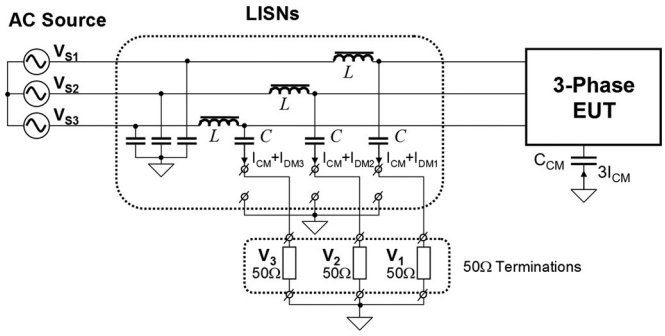

Fig. 1. EMI noise measurement setup for a three-phase power electronics system.

$\mathbf{I_{DM3}}$ also flow through LISNs and 50 Ω terminations. It should be pointed out that there are two different definitions on CM noise current in the literature [2], [9]–[18]. For the first definition, the total CM noise of all lines is defined as $I_{\rm CM}$; and for the second definition, the CM noise of each line is defined as $I_{\rm CM}$. This paper will use the second definition because the second definition is more convenient for the EMI analysis, measurement, and diagnosis, and furthermore, it agrees with the definition of DM noise. The 50 Ω terminations can either be the input impedances of a spectrum analyzer or standard 50 Ω terminators. Since the EMI standards concern the noise voltage drop on 50 Ω terminations, this paper addresses the CM and DM noise current flowing through the 50 Ω terminations only. The noise flowing through the inductor L_s in the LISNs is not discussed here. The CM or DM noise voltage drop on a 50-Ω termination is $I_{\rm CM}$ 50 Ω or $I_{\rm DM}$ 50 Ω. They are defined as DM or CM noise voltage. The convenience of the second CM noise definition is obvious here. For the first definition, the CM noise voltage drop on a 50 Ω termination is $I_{\rm CM}$(50 Ω/*n*), where *n* is the number of phase, so its math expression does not agree with $I_{\rm DM}$ 50 Ω of the DM noise voltage drop. It will be shown later that the second CM noise definition is more convenient for the EMI measurement and diagnosis because the noise voltage drop measured by a spectrum analyzer on a 50 Ω termination is equal to the vector sum or the vector difference of the DM and CM noise voltage drops, $I_{\rm DM}$ 50 Ω and $I_{\rm CM}$ 50 Ω. As a comparison, for the first definition, the noise voltage drop measured by a spectrum analyzer on a 50 Ω termination is the vector sum or the vector difference of $I_{\rm DM}$ 50 Ω and $I_{\rm CM}$(50 Ω/*n*). There is a variable *n* in it, so the CM noise voltage needs to be converted based on the number of phase. Because of these, all the analysis in this paper is based on the second definition of the CM noise current.

In Fig. 1, the noise voltage drop $\mathbf{V}_1$, $\mathbf{V}_2$, or $\mathbf{V}_3$ on one of the 50 Ω terminations is defined as the total noise on phase 1, 2, or 3, and it is the vector sum of CM and DM noise voltages on each phase. The CM and DM noise voltages can then be calculated from

$$|\mathbf{V_{CM}}| = \left|\frac{\mathbf{V}_1+\mathbf{V}_2+\mathbf{V}_3}{3}\right| = 50\,|\mathbf{i_{CM}}| \tag{1}$$

$$|\mathbf{V_{DM1}}| = |\mathbf{V}_1-\mathbf{V_{CM}}| = \left|\frac{2\mathbf{V}_1-\mathbf{V}_2-\mathbf{V}_3}{3}\right| = 50\,|\mathbf{i_{DM1}}| \tag{2}$$

$$|\mathbf{V_{DM2}}| = |\mathbf{V}_2-\mathbf{V_{CM}}| = \left|\frac{2\mathbf{V}_2-\mathbf{V}_1-\mathbf{V}_3}{3}\right| = 50\,|\mathbf{i_{DM2}}| \tag{3}$$

$$|\mathbf{V_{DM3}}| = |\mathbf{V}_3-\mathbf{V_{CM}}| = \left|\frac{2\mathbf{V}_3-\mathbf{V}_1-\mathbf{V}_2}{3}\right| = 50\,|\mathbf{i_{DM3}}|\,. \tag{4}$$

For an *n*-phase ($n \geq 2$) system, the CM noise and the DM noise for the phase *p* can be defined similarly to a three-phase system as

$$|\mathbf{V_{CM}}| = \left|\frac{\sum_{k=1}^{n}\mathbf{V}_k}{n}\right| = 50\,|\mathbf{i_{CM}}| \tag{5}$$

$$|\mathbf{V_{DM}}p| = |\mathbf{V}_p-\mathbf{V_{CM}}| = \left|\frac{n\mathbf{V}_p-\sum_{k=1}^{n}\mathbf{V}_k}{n}\right| = 50\,|\mathbf{i_{DM}}p| \tag{6}$$

where $2 \leq p \leq n$, $\mathbf{V}_k$ is the noise voltage on the phase *k*, and $\mathbf{V}_p$ is the noise voltage on the phase *p*. It should be noted that a conventional single-phase power electronics system is a two-phase system for EMI noise because there are DM and CM noises on both lines and their reference is the ground. Because of this, $n \geq 2$.

Based on symmetrical component theory [19], an *n*-phase voltage set can be decomposed into a zero-sequence voltage set ($\mathbf{V}^0$, $\mathbf{V}^0$, ... ,$\mathbf{V}^0$) consisting of *n* equal vectors, and $n-1$ sequence voltage sets ($\mathbf{V_1^1}$, $\mathbf{V_2^1}$, ... ,$\mathbf{V}_n^1$), ($\mathbf{V_1^2}$, $\mathbf{V_2^2}$, ... ,$\mathbf{V}_n^2$), ... ($\mathbf{V_1^{n-1}}$, $\mathbf{V_2^{n-1}}$, ... ,$\mathbf{V}_n^{n-1}$) consisting of *n* equispaced vectors, where $\mathbf{V}^0$ is the zero-sequence voltage vector and $\mathbf{V}_p^m$ is the *m*th sequence voltage vector of phase *p*. $\mathbf{V}^0$ can be calculated in

$$\mathbf{V^0} = \frac{1}{n}\sum_{k=1}^{n}\mathbf{V}_k = \mathbf{V_{CM}}. \tag{7}$$

Zero-sequence voltage is, therefore, equal to the CM voltage in (7). $\mathbf{V}_p^m$ can be calculated in

$$\mathbf{V}_p^m = \frac{1}{n}\left(\sum_{k=1}^{n}\mathbf{V}_k e^{j\frac{2m(k-1)\pi}{n}}\right)\left(e^{-j\frac{2m(p-1)\pi}{n}}\right), \quad m \in [1, n-1], \qquad p \in [1, n]. \tag{8}$$

The noise voltage $\mathbf{V}_p$ on phase *p* is equal to the sum from zero sequence to $(n-1)$th sequence voltages

$$\mathbf{V}_p = \frac{1}{n}\sum_{k=1}^{n}\mathbf{V}_k + \frac{1}{n}\sum_{m=1}^{n-1}\left[\left(\sum_{k=1}^{n}\mathbf{V}_k e^{j\frac{2m(k-1)\pi}{n}}\right) \times \left(e^{-j\frac{2m(p-1)\pi}{n}}\right)\right], \qquad p \in [1, n]. \tag{9}$$

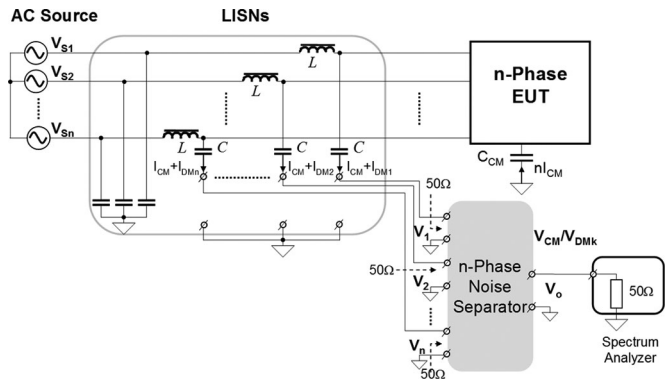

Fig. 2. Using an *n*-phase noise separator to separate DM and CM noise.

The DM noise of the phase *p* is therefore

$$\mathbf{V_{DM}}_p = \mathbf{V}_p - \mathbf{V_{CM}} = \frac{1}{n}\sum_{m=1}^{n-1}\left[\left(\sum_{k=1}^{n}\mathbf{V}_k e^{j\frac{2m(k-1)\pi}{n}}\right)\times\left(e^{-j\frac{2m(p-1)\pi}{n}}\right)\right], p\in[1,\ n]. \tag{10}$$

From (10), the DM noise of each phase is the sum from first to $(n-1)$th sequence voltages.

If $\boldsymbol{V} = (\mathbf{V}_1, \mathbf{V}_2, \ldots, \mathbf{V}_n)$, $\boldsymbol{V}^0 = (\mathbf{V}^0, \mathbf{V}^0, \ldots, \mathbf{V}^0)$, and $\boldsymbol{V}^m = (\mathbf{V}_1^m, \mathbf{V}_2^m, \ldots, \mathbf{V}_n^m)$,

$$\boldsymbol{V} = \boldsymbol{V}^0 + \sum_{m=1}^{n-1}\boldsymbol{V}^m \tag{11}$$

$$\mathbf{V_{CM}} = \boldsymbol{V}^{\mathbf{0}} \tag{12}$$

$$\mathbf{V}_{\mathbf{DM}}^m = \boldsymbol{V}^m \tag{13}$$

$\mathbf{V}_{\mathbf{DM}}^{\mathbf{m}}$ is the *m*th sequence DM noise set and *m* is from 1 to $n-1$.

III. Characterization of *n*-Phase Noise Separators

A. Transmission and Rejection Ratios of a Multiphase Noise Separator

Fig. 2 shows an EMI noise measurement setup with an *n*-phase noise separator. There are *n* input ports and one output port. The *n* input ports have 50 Ω input impedances terminating LISNs. The output is terminated by the 50 Ω input impedance of a spectrum analyzer. The output of the noise separator could be the CM noise $V_{\rm CM}$, and the DM noise $V_{\rm DMn}$ for phase *n*.

In order to separate DM and CM noises, the noise separator should satisfy three requirements.

1) Input impedances are always real 50 Ω and are independent from noise source impedances.
2) The output of the CM noise separator is $\frac{1}{n}\sum_{k=1}^{n}\mathbf{V}_k$. The output of the DM noise separator for phase *n* is
$$\frac{1}{n}\sum_{m=1}^{n-1}\left[\left(\sum_{k=1}^{n}\mathbf{V}_k e^{j\frac{2m(k-1)\pi}{n}}\right)\left(e^{-j\frac{2m(p-1)\pi}{n}}\right)\right], p\in[1,n].$$
3) Leakage between the CM and the DM at the output should be small.

Requirement 1) guarantees consistent measurement conditions and accurate sampling of noise voltage; 2) guarantees correct noise separation; and 3) guarantees small interference between the CM and DM noise measurements.

The first requirement can be characterized using network parameters, such as the reflection coefficient in wave theory. The second requirement can be characterized by the transmission coefficient of noise separators. The DM transmission ratio DMTR_p^m of the *m*th sequence DM noise on phase *p* and the CM transmission ratio (CMTR) for the CM noise are the parameters that need to be characterized and evaluated.

DMTR_p^m and CMTR are defined as follows:

$$\text{for CM noise separator: } \mathrm{CMTR} = \frac{\mathbf{V}_{\mathrm{CM\_out}}}{\mathbf{V}_{\mathrm{CM\_in}}} \tag{14}$$

$$\text{for DM noise separator: } \mathrm{DMTR}_p^m = \frac{\mathbf{V}_{\mathrm{DM\_out}\_p}^m}{\mathbf{V}_{\mathrm{DM\_in}\_p}^m}. \tag{15}$$

In (14), $\mathbf{V}_{\mathbf{CM\_in}}$ is the CM voltage excitation set fed to the inputs of a CM noise separator. The CM voltage excitation is added to each input port. $\mathbf{V}_{\mathbf{CM\_out}}$ is the voltage response at the output of this CM noise separator due to $\mathbf{V}_{\mathbf{CM\_in}}$. In (15), the *m*th sequence DM voltage excitation set $\mathbf{V}_{\mathrm{DM\_in}}^m$ is fed to the inputs of a DM noise separator. $\mathbf{V}_{\mathrm{DM\_in}\_p}^m$ is the *m*th sequence DM noise voltage excitation added to phase *p*. $\mathbf{V}_{\mathrm{DM\_out}\_p}^m$ is the *m*th sequence DM voltage response on phase *p* at the output of this DM noise separator due to $\mathbf{V}_{\mathrm{DM\_in}}^m$. From (14) and (15), it can be seen that an ideal CMTR or DMTR_p^m should be 0 dB. Because DM noise is the sum of $n-1$ sequence DM noise voltage sets, the phase of each DMTR_p^m should be the same.

Requirement 3) can be characterized by parameters: the DM rejection ratio DMRR^m to the *m*th sequence DM voltage excitation set at CM output and the CM rejection ratio CMRR_p to the CM noise at the DM output of phase *p*. They are defined as

$$\text{for CM noise separator: } \mathrm{DMRR}^m = \frac{\mathbf{V}_{\mathrm{CM\_out}}^m}{\mathbf{V}_{\mathrm{DM\_in\_1}}^m}, \text{ and} \tag{16}$$

$$\text{for DM noise separator: } \mathrm{CMRR}_p = \frac{\mathbf{V}_{\mathrm{DM\_out}\_p}}{\mathbf{V}_{\mathrm{CM\_in}}} \tag{17}$$

where the *m*th sequence DM noise set $\mathbf{V}_{\mathbf{DM\_in}}^m$ is fed to the inputs of a CM noise separator and $\mathbf{V}_{\mathbf{CM\_out}}^m$ is the voltage response at the output of this CM noise separator due to $\mathbf{V}_{\mathrm{DM\_in}}^m$. DMRR^m is defined as the ratio of $\mathbf{V}_{\mathbf{CM\_out}}^m$ to $\mathbf{V}_{\mathrm{DM\_in\_1}}^m$, the *m*th sequence DM noise in the input of phase 1. It should be pointed out that the only difference between two *m*th sequence DM noise voltages on two different inputs is their phase angles, so $\mathbf{V}_{\mathrm{DM\_in\_1}}^m$ is used to represent $\mathbf{V}_{\mathrm{DM\_in}}^m$ in (16). $\mathbf{V}_{\mathbf{CM\_in}}$ is the CM voltage set fed to the inputs of a DM noise separator, and $\mathbf{V}_{\mathrm{DM\_out}\_p}$ is the output voltage in phase *p* of this DM noise separator due to $\mathbf{V}_{\mathbf{CM\_in}}$. DMRR^m and CMRR_p should be as small as possible. Additionally, an *n*-phase DM noise separator has a CMRR_p for each phase and an *n*-phase CM noise separator has $n-1$ different DMRR^m.

For any noise voltage set added to the inputs of an *n*-phase noise separator, the noise voltage can always be decomposed to CM noise and $n-1$ sequence DM noise. The outputs of the

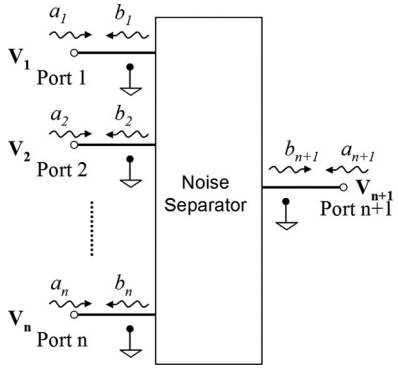

Fig. 3. Characterizing an n-phase noise separator in terms of waves.

noise separator are given by

$$\mathbf{V}_{\mathrm{CM\_out}} = \mathrm{CMTR} \times \mathbf{V}_{\mathrm{CM\_in}} + \sum_{m=1}^{n-1} \left(\mathrm{DMRR}^m \times \mathbf{V}^m_{\mathrm{DM\_in\_1}}\right) \tag{18}$$

$$\mathbf{V}_{\mathrm{DM\_out\_}p} = \sum_{m=1}^{n-1} \left(\mathrm{DMTR}^m_p \times \mathbf{V}^m_{\mathrm{DM\_in\_}p}\right) + \mathrm{CMRR}_p \times V_{\mathrm{CM\_in}}. \tag{19}$$

Appropriate network parameters need to be introduced to characterize and evaluate the noise separators according to the three requirements. Scattering parameters (S-parameters) are selected in this paper for three reasons. First, frequency-domain characterization of a network employing [*Z*], [*Y*], [*H*], and [*ABCD*] parameters often requires either a short circuit or an open circuit at one port, which is difficult to achieve in the high-frequency (HF) range because of parasitic parameters [3], [4]. On the other hand, for S-parameters no short or open circuit is needed. Second, the S-parameter method can be calibrated to the exact points of measurement so that the effects of parasitics due to measurement interconnects are excluded. For [*Z*], [*Y*], [*H*], and [*ABCD*] parameters' measurement, expensive special probes may be needed for calibration. Third, S-parameters are analytically convenient and capable of providing a great insight into a measurement or design problem [4]. Because of the S-parameters, the powerful signal-flow graph can be used for network analysis with clear physical concepts.

It should be pointed out that because the DM noise added to the noise separator has $2(n-1)$ DOF, any methods using an excitation with fewer than $2(n-1)$ DOF cannot offer a full evaluation for DMTR and DMRR.

B. Characterization of Noise Separators Using S-Parameters

For a CM or DM n-phase noise separator in Fig. 2, there are n input ports and one output port; therefore, it is a $(n+1)$-port network. This $(n+1)$-port linear passive network can be characterized in terms of waves, as shown in Fig. 3.

In Fig. 3, a_i is the normalized incident wave, and b_i is the normalized reflected wave. Port voltage $\mathbf{V}_i$ can be expressed by [5], [6]

$$\mathbf{V}_i = \sqrt{Z_0}(a_i + b_i) \tag{20}$$

where Z_0 is the reference impedance, which is usually 50 Ω, and i is the port number from 1 to $n+1$.

To fully characterize an $(n+1)$-port linear passive network, $(n+1)$ linear equations are required among the $2(n+1)$ wave variables [11]. The $(n+1)^2$ S-parameters in (21) are, therefore, introduced to correlate a_i and b_j [5], [7]. S_{ii} refers to the reflection coefficients, and S_{ij} represents the transmission coefficients. Both i and j are port numbers from 1 to $n+1$

$$\begin{pmatrix} b_1 \\ b_2 \\ \vdots \\ b_{n+1} \end{pmatrix} = \begin{pmatrix} S_{11} & S_{12} & \cdots & S_{1(n+1)} \\ S_{21} & S_{22} & \cdots & S_{2(n+1)} \\ \vdots & \vdots & \ddots & \vdots \\ S_{(n+1)1} & S_{(n+1)2} & \cdots & S_{(n+1)(n+1)} \end{pmatrix} \times \begin{pmatrix} a_1 \\ a_2 \\ \vdots \\ a_{n+1} \end{pmatrix} \Rightarrow [b] = [S][a]. \tag{21}$$

According to the transmission-line theory [5], [8], when the reflected wave b_j reaches the source or load side, it will also be reflected because of the mismatched impedances. The reflection coefficients Γ_{sk} at the source side and Γ_L at the load side are given in (22) and (23), respectively. In (22), k is from 1 to n. It is known that for passive networks $|\Gamma_{sk}| \le 1$ and $|\Gamma_L| \le 1$

$$\Gamma_{sk} = \frac{Z_{sk} - Z_0}{Z_{sk} + Z_0}, \text{ and} \tag{22}$$

$$\Gamma_L = \frac{Z_L - Z_0}{Z_L + Z_0}. \tag{23}$$

Fig. 3 is then characterized by the signal-flow graph in Fig. 4. In Fig. 4, b_{sk} is the normalized wave emanating from the source. For a given voltage source $\mathbf{V}_{sk}$ with source impedance Z_{sk}, b_{sk} is given by [8]

$$b_{sk} = \frac{\sqrt{Z_0}\mathbf{V}_{sk}}{Z_{sk} + Z_0}. \tag{24}$$

Because the output of the noise separator is terminated by the 50 Ω input impedance of the spectrum analyzer, as shown in Fig. 2, the reflection coefficient Γ_L is zero. As a result, a_{n+1} is zero, and the signal-flow graph is equivalent to Fig. 5. Fig. 5 characterizes a practical noise separator matched by a spectrum analyzer at the output port. It is now important to determine the appropriate **S** matrix for an ideal noise separator.

In order to achieve 50 Ω input impedances independent from noise source impedances, the reflection coefficients at input ports must be zero. In Fig. 5, using Mason's rule, the reflection coefficient Γ_k *is* described as

$$\Gamma_k = \frac{Z_{\mathrm{ink}} - Z_0}{Z_{\mathrm{ink}} + Z_0} = S_{kk} + \Delta_k \tag{25}$$

where Z_{ink} is the input impedances of port k and Δ_k is the equivalent input reflection coefficient of port k excluding the effects of S_{kk}. From (25), it is obvious that in order to guarantee 50 Ω input impedances independent from noise source impedances,

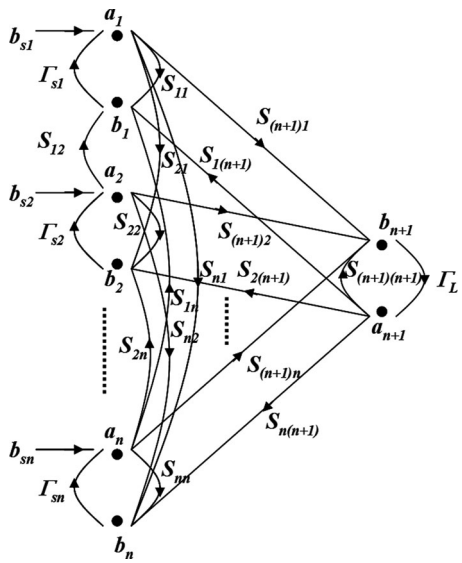

Fig. 4. Characterizing the noise separator using a signal-flow graph.

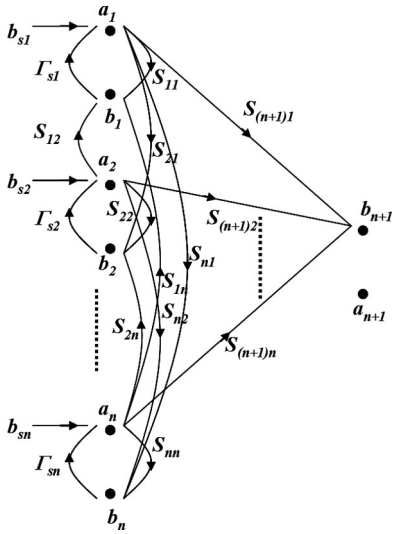

Fig. 5. Signal-flow graph of a noise separator terminated with a 50-Ω input impedance of a spectrum analyzer.

S_{kq} must be zero; as a result, b_k is zero, where k and q are from 1 to n. The signal-flow graph is, thus, equivalent to Fig. 6.

In Fig. 6, based on (20) and (21), the voltage at the output port is given by

$$\mathbf{V}_{n+1} = \sum_{k=1}^{n} \mathbf{V}_k \mathbf{S}_{(n+1)k}. \tag{26}$$

Based on (5) and (26), for a CM noise separator

$$S_{(n+1)p} = \frac{1}{n}, \qquad S_{(n+1)p} = -\frac{1}{n}, \qquad p \in [1, n]. \tag{27}$$

Based on (6) and (26), for the DM noise separator of phase p

$$S_{(n+1)p} = \frac{n-1}{n}, \qquad S_{(n+1)q} = -\frac{1}{n}, \qquad q \in [1, \ldots, p-1, p+1, \ldots, n] \tag{28}$$

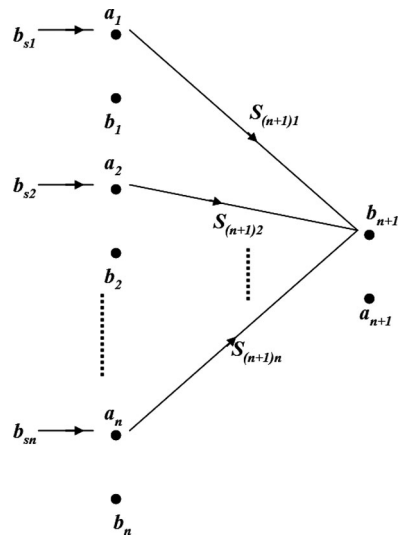

Fig. 6. Signal-flow graph for an ideal n-phase noise separator with a matched load at output port.

or

$$S_{(n+1)p} = -\frac{n-1}{n}, \qquad S_{(n+1)q} = \frac{1}{n}, \qquad q \in [1, \ldots, p-1, p+1, \ldots, n].$$

The final **S** matrix for an ideal CM noise separator is therefore

$$[\mathbf{S}] = \begin{pmatrix} 0 & 0 & \cdots & S_{1(n+1)} \\ 0 & 0 & \cdots & S_{2(n+1)} \\ \vdots & \vdots & \ddots & \vdots \\ \pm\dfrac{1}{n} & \pm\dfrac{1}{n} & \cdots & S_{(n+1)(n+1)} \end{pmatrix}. \tag{29}$$

The **S** matrix for the ideal DM noise separator of phase p is (30). In (29) and (30), the last column of the **S** matrix is independent of the performance of a noise separator because the output port $n+1$ is matched; therefore, there is no output impedance requirement

$$[\mathbf{S}] = \begin{pmatrix} 0 & \cdots & 0 & 0 & 0 & \cdots & S_{1(n+1)} \\ \vdots & \ddots & \cdots & \cdots & \cdots & \cdots & S_{2(n+1)} \\ \vdots & \vdots & \ddots & \cdots & \cdots & \cdots & \vdots \\ \vdots & \vdots & \vdots & \ddots & \cdots & \cdots & \vdots \\ \vdots & \vdots & \vdots & \vdots & \ddots & \cdots & \vdots \\ 0 & \vdots & 0 & 0 & 0 & \ddots & S_{n(n+1)} \\ \mp\dfrac{1}{n} & \cdots & \mp\dfrac{1}{n} & \pm\dfrac{n-1}{n} & \mp\dfrac{1}{n} & \cdots & S_{(n+1)(n+1)} \end{pmatrix}. \tag{30}$$

For a practical noise separator, the S-parameters are not exactly equal to the values defined in (29) and (30), so Fig. 5 should be used for evaluation. The input impedance of a noise separator can be evaluated through (25). In (25), the second term can be ignored if it is much smaller than the first term, which indicates that the input impedances are independent from Γ_{sk}, which represent the source impedances. Then, the input impedances

can be characterized solely by S_{kk} and are free of noise source impedances in

$$Z_{ink} = Z_0 \frac{1+\Gamma_k}{1-\Gamma_k} \approx Z_0 \frac{1+S_{kk}}{1-S_{kk}}. \tag{31}$$

Based on (14), a CM voltage excitation set $\mathbf{V}_{\mathbf{CM\_in}}$ is fed to the input ports. There is a CM voltage response $\mathbf{V}_{\mathbf{CM\_out}}$ at the output due to $\mathbf{V}_{\mathbf{CM\_in}}$. It should be pointed out that no DM excitations can be added to the derivation of CMTR since the on-ideal DMRR will lead to CM responses at the output. The CMTR is the voltage ratio of $\mathbf{V}_{\mathbf{CM\_out}}$ to $\mathbf{V}_{\mathbf{CM\_in}}$. Because the CM voltage excitation added to each input port is equal, based on (20)

$$V_1 = V_i = V_{\mathrm{CM\_in}}, \quad i \in [2, n] \tag{32}$$

$$V_{n+1} = V_{\mathrm{CM\_out}} \tag{33}$$

$$(a_1 + b_1) = (a_i + b_i), \quad i \in [2, n] \tag{34}$$

Based on (34), Fig. 5, and Mason's rule

$$\frac{b_1}{a_1} = S_{11} + \Delta_1 \tag{35}$$

$$\frac{b_i}{a_i} = S_{ii} + \Delta_i \tag{36}$$

$$\frac{a_i}{a_1} = \frac{1 + S_{11} + \Delta_1}{1 + S_{ii} + \Delta_i} \tag{37}$$

$$\begin{aligned} b_{n+1} &= a_1 S_{(n+1)1} + \sum_{i=2}^{n} \left(a_i S_{(n+1)i}\right) \\ &= a_1 \left[S_{(n+1)1} + \sum_{i=2}^{n} \left(\frac{a_i}{a_1} S_{(n+1)i} \right) \right] \\ &= a_1 \left[S_{(n+1)1} + \sum_{i=2}^{n} \left(\frac{1 + S_{11} + \Delta_1}{1 + S_{ii} + \Delta_i} S_{(n+1)i} \right) \right] \end{aligned} \tag{38}$$

So, based on (14), (32), (33), (35), and (38)

$$\begin{aligned} \mathrm{CMTR} = \frac{V_{n+1}}{V_1} &= \frac{\sqrt{Z_0} b_{n+1}}{\sqrt{Z_0}(a_1 + b_1)} = \frac{\frac{b_{n+1}}{a_1}}{1 + \frac{b_1}{a_1}} \\ &= \frac{S_{(n+1)1} + \sum_{i=2}^{n} \left(\frac{1+S_{11}+\Delta_1}{1+S_{ii}+\Delta_i} S_{(n+1)i} \right)}{1 + S_{11} + \Delta_1} \\ &= \sum_{k=1}^{n} \left(\frac{S_{(n+1)k}}{1 + S_{kk} + \Delta_k} \right). \end{aligned} \tag{39}$$

For a good CM noise separator, the magnitude of CMTR should be close to 0 dB.

The derivation processes for DM transmission ratios, CM rejection ratios, and DM rejection ratios are similar to the derivation process of CMTR shown earlier. For DM transmission ratios and rejection ratios, the excitations are DM sequence voltage sets, so the phase relationship of input voltages should be considered during the derivation process for different sequence voltage excitations. Based on (15), (20), and Fig. 5, the DMTR_p^m for a DM noise separator can be derived using Mason's rule in (40).

For a DM noise separator, the *m*th sequence DM transmission ratio of phase *p* is

$$\mathrm{DMTR}_p^m = \sum_{k=1}^{n} \left(\frac{S_{(n+1)k}}{(1 + S_{kk} + \Delta_k)} e^{-j\frac{2m(k-p)\pi}{n}} \right). \tag{40}$$

As analyzed in the previous section, both magnitude and phase are important for DMTR_p^m because the output of the DM noise separator is the vector sum of the $n-1$ sequence voltage vectors. For a good DM noise separator, the magnitudes of DMTR_p^m should be close to 0 dB, and their phases should be the same so that the vector sum of the $n-1$ sequences would not be changed at each frequency.

Based on (16), (17), (20), Fig. 5, and the symmetrical component theory, the DMRR^m for the CM noise separator and the CMRR_p for the DM noise separator can be derived as follows:

$$\mathrm{DMRR}^m = \sum_{k=1}^{n} \left(\frac{S_{(n+1)k}}{(1 + S_{kk} + \Delta_k)} e^{-j\frac{2m(k-1)\pi}{n}} \right) \tag{41}$$

$$\mathrm{CMRR}_p = \sum_{k=1}^{n} \frac{S_{(n+1)k}}{(1 + S_{kk} + \Delta_k)} \approx \sum_{k=1}^{n} \frac{S_{(n+1)k}}{(1 + S_{kk})}. \tag{42}$$

In (41) and (42), *p* is the phase number from 1 to *n*.

Equations (25), (31), and (39)–(42) are critical for *n*-phase noise-separator evaluation. For an *n*-phase noise separator, as long as the S-parameters are measured using a network analyzer, its performance can be evaluated using (25), (31), and (39)–(42). In (25), if the second terms are much smaller than the first terms, the input impedances are independent of noise source impedances.

IV. Design a Multiphase Noise Separator

This section first proposes a function scheme for *n*-phase noise separators based on the theory developed in Sections II and III. The circuit, which can realize the function scheme, is proposed, and its design technique is explored. Finally, as an example, a three-phase noise separator is built with the proposed design technique.

A. Proposed Circuit Structure for Multiphase Noise Separators

Based on the analysis in the previous section, the CM noise is the zero-sequence noise, and the DM noise is the sum of all $n-1$ sequence noises. An *n*-phase noise separator can be designed in three steps based on this principle. In the first step, a network that can separate all $n-1$ sequence noises from zero-sequence noise is developed. The network can also add all sequence noises together at its outputs. Furthermore, it can provide 50 Ω input impedances for all $n-1$ sequence noises, and infinite input impedance for zero-sequence noise. In the second step, another network which can separate zero-sequence noise from $n-1$ sequence noises is developed. The network should also provide a 50 Ω input impedance for zero-sequence noise and infinite input impedances for all $n-1$ sequence noises. In the last step, the inputs of these two networks are connected in parallel. Based on the network theory, the combined network can achieve both

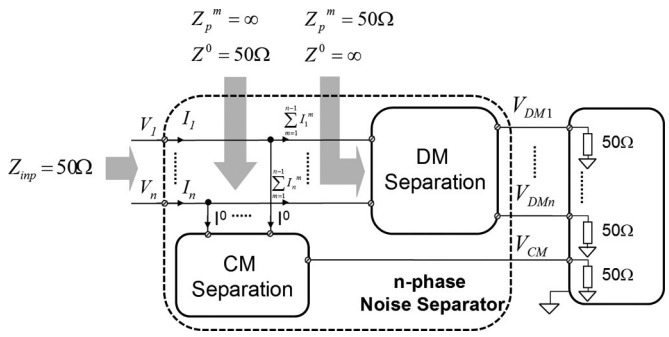

Fig. 7. Circuit structure for the proposed n-phase noise separator.

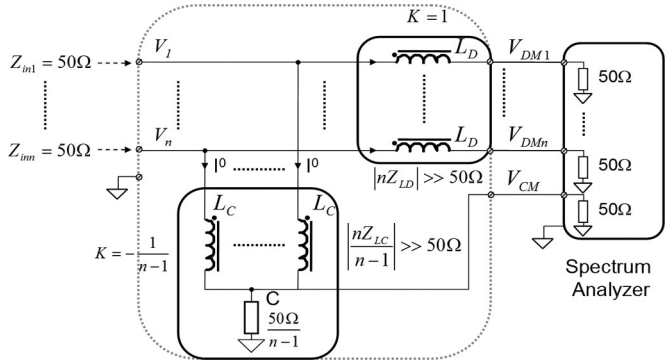

Fig. 8. Proposed circuit for n-phase noise separators.

noise separation and 50 Ω input impedances for any noise. Fig. 7 shows this concept.

In Fig. 7, the DM separation unit has 50 Ω input impedances Z_p^m for sequence noise. It can conduct sequence noise to a 50 Ω load without attenuation. At the same time, the unit has very high impedance Z^0 for zero-sequence noise, and it does not conduct the zero-sequence noise to the 50 Ω load. The unit can, therefore, separate the DM noise for each phase. The CM separation unit is a different story. It has a 50-Ω impedance Z^0 for zero-sequence noise and can conduct the zero-sequence noise to a 50-Ω load without attenuation. At the same time, it has very high impedances Z_p^m for sequence noise. It does not conduct sequence noises to the 50-Ω load. The CM separation unit can thus separate CM noise from the DM noise. Because the DM separation unit has a 50 Ω input impedance for sequence noises and the CM separation unit has a 50 Ω input impedance for zero-sequence noise, the combined input impedance of each phase is 50 Ω, which can be proved in

$$Z_{\text{inp}} = \frac{V_p}{I_p} = \frac{V^0 + \sum_{m=1}^{n-1} V_p^m}{I^0 + \sum_{m=1}^{n-1} I_p^m} = \frac{50I^0 + \sum_{m=1}^{n-1} 50I_p^m}{I^0 + \sum_{m=1}^{n-1} I_p^m} = 50\ \Omega. \tag{43}$$

In (43), p is the input port number from 1 to n.

B. Circuit Design for Multiphase Noise Separators

Fig. 8 shows the circuit being proposed to achieve the function of an n-phase noise separator. The DM separation unit has n identical inductors with inductance L_D ideally coupled. For the CM current, the decoupled impedance of each inductor is nZ_{LD}, which is larger than 50 Ω. This approximately meets the condition of infinite CM impedance. Because the inductors are ideally coupled, the magnetic fields generated by symmetrical sequence currents in the core are canceled. The inductance for DM currents is zero. The DM input impedances are, therefore, equal to load impedance 50 Ω. The DM noise is directly added to the loads.

The CM separation unit has n identical inductors L_C coupled. The coupling coefficient between any two inductors is designed to be $-1/(n-1)$. The decoupled inductance to sequence noise is $|nL_C/(n-1)|$. Its impedance $|nZ_{LC}/(n-1)|$ should be much larger than 50 Ω to achieve high DM input impedances. The structure is symmetrical to sequence noise, so the DM voltage at center point C is zero. Because the coupling coefficient is $-1/(n-1)$, the magnetic fields generated by CM currents are canceled inside the core. The CM inductance is zero and the CM noise is directly added to load and the grounded resistance 50 Ω/$(n-1)$. Because the grounded resistance is in parallel with the 50-Ω load, the paralleled resistance is 50 Ω/n. The equivalent CM input impedance to each input is 50 Ω.

In Fig. 8, for DM separation unit, if the inductor's coupling coefficient K is smaller than 1, there is leakage inductance on each phase. At high frequencies, the impedance could be significant, so the input impedance will deviate from 50 Ω and the DM noise will be attenuated. Because of this, coupling coefficient K should be as close to unity as possible. It is possible to design the coupled inductors using a transmission line transformer so that the effects of the leakage inductance can be canceled by the capacitance between windings when the characteristic impedance of the multiconductor transmission line is equal to 50 Ω. For CM separation unit, the coupling coefficient should be as close to $-1/(n-1)$ as possible to avoid any attenuation due to leakage inductance. Inductors should be as identical as possible to improve DM rejection ratios.

C. Prototype Development

Based on the analysis in Section III, to build a high-performance noise separator, the coupled inductors in the DM separation unit should meet the following conditions.

1) Inductance L_D should be large enough so that $|nZ_{LD}|$ has impedance much higher than 50 Ω within the concerned frequency range, so a good CMRR can be achieved.
2) Leakage inductance should be small enough so that the inductor has DM impedance much smaller than a 50-Ω load, so a good DMTR can be achieved.

A high-permeability ferrite toriodal core can be used for the inductor design. An n-filar winding structure can be employed to achieve a high coupling coefficient. For an n-filar winding structure, the n pieces of wires are almost at the same position, so the leakage energy is only stored in the air gaps between the wires. A low leakage inductance is achieved. To further reduce the effects of leakage inductance on DMTRs, the characteristic impedance of the n-conductor transmission line is designed to be 50 Ω so that the effects of leakage inductance and the winding

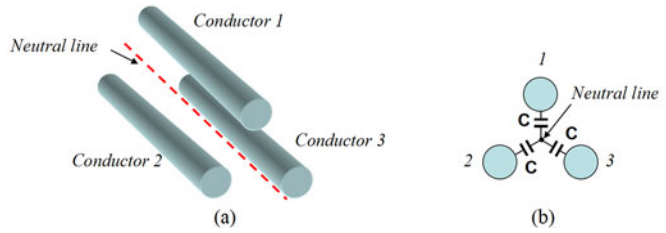

Fig. 9. Three-conductor transmission line. (a) Neutral line and (b) Capacitance C.

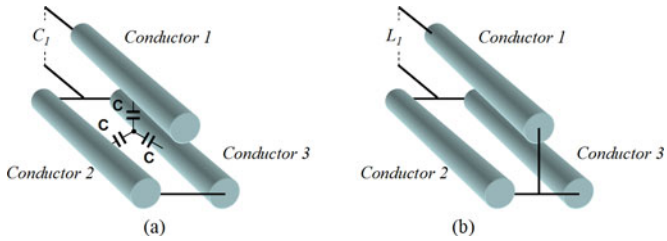

Fig. 10. Measurement of three-conductor transmission line parameters. (a) Open capacitance C_1 and (b) Short inductance L_1.

capacitance between windings are canceled. The impedance of the inductor should be much higher than 50 Ω. If the coupled inductor does not have enough bandwidth due to parasitic winding capacitance, two or more coupled inductors can be built for different frequency ranges.

Fig. 9(a) shows a three-conductor transmission line. Because three conductors have a symmetric structure and all sequence noise excitations are symmetric, there is a virtual neutral line with a 0-V potential as shown in Fig. 9. Each conductor is a transmission line reference to the neutral line. The characteristic impedance of a single transmission line can be described using a conventional transmission line theory. Ignoring the power loss, the characteristic impedance is given by (44). In (44), L and C are the inductance and capacitance per unit length to the neutral line. Fig. 9(b) shows the capacitance C. To find the characteristic impedance of each transmission line, any two conductors are shorted together at both ends. The open capacitance C_1 between the third conductor and the two shorted conductors is measured as shown in Fig. 10(a). The short inductance L_1 between the third conductor and the two shorted conductors with all the other ends shorted is measured in Fig. 10(b)

$$Z_0 = \sqrt{\frac{L}{C}}. \tag{44}$$

It can be proved that the characteristic impedance of the single transmission line is given by

$$Z_0 = \sqrt{\frac{L}{C}} = \frac{1}{2}\sqrt{\frac{L_1}{C_1}}. \tag{45}$$

In experiments, for a three-phase example, a high-permeability ferrite toriodal core, ZJ42206TC (J material from Magnetics Inc., Pittsburgh, PA), is used for the inductor design. A 30-turn trifilar winding structure is employed to achieve a high coupling coefficient. The measured $|3Z_{LD}|$ is larger than 8.7 kΩ from 150 kHz to 10 MHz, so it is much larger than 50 Ω.

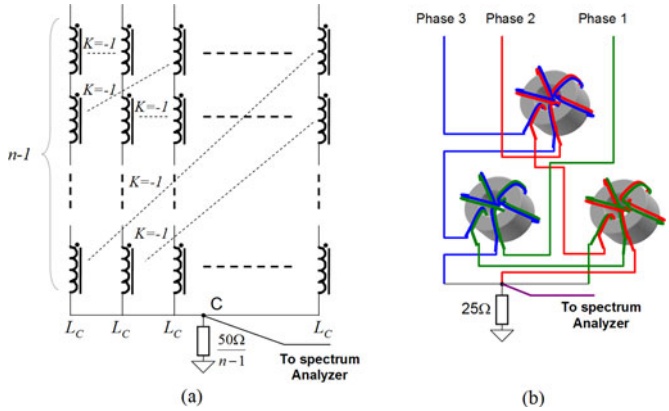

Fig. 11. n-phase CM separation unit with $n(n-1)/2$ identical coupled inductors. (a) Circuit and (b) Three-phase example.

The measured coupling coefficient between any two windings is 0.99995, which is derived from the measured leakage inductance and magnetizing inductance; and the measured leakage inductance for the first and second sequence noises is 174 nH. The noise separator is designed to work from 150 kHz to 10 MHz. At 10 MHz, 174 nH leads to an 11-Ω DM impedance, so it is not negligible compared with a 50-Ω load. The measured characteristic impedance for the first and the second sequence noises is 43.3 Ω, which is close to 50 Ω, so the effect of leakage inductance is greatly reduced.

To find the characteristic impedance of an n-conductor transmission line with a symmetric structure, similar to three-conductor transmission lines, any $n-1$ conductors are shorted together at both of their ends. The open capacitance C_1 between the nth conductor and the $n-1$ shorted conductors is measured. The short inductance L_1 between the nth conductor and the $n-1$ shorted conductors with all the other ends shorted is also measured. The characteristic impedance of a single transmission line is

$$Z_0 = \frac{1}{2}\sqrt{\frac{L_1}{C_1}}. \tag{46}$$

For the CM separation unit, the coupled inductors should meet the following conditions.

1) L_C should be large enough so that $|nZ_{LC}/(n-1)|$ has impedance much higher than 50 Ω within the concerned frequency range. This helps the noise separator to achieve a 50-Ω input impedance for DM noise.
2) The inductors should be as balanced as possible, and the coupling coefficient between two phases should be as close to $-1/(n-1)$ as possible. This condition guarantees that the noise separator has a good CMTR and DMRR.

Fig. 11(a) shows the method to build a coupled inductor using $n(n-1)/2$ identical inductors for a n-phase CM separation unit. In Fig. 11(a), each inductor has two windings closely coupled with a coupling coefficient of -1. There are total $n(n-1)$ windings on $n(n-1)/2$ inductors. The $n(n-1)/2$ inductors are connected in such a way that the inductor L_C on each phase in Fig. 8 includes $n-1$ series windings on $n-1$ different inductors, and these $n-1$ windings are inversely coupled to the

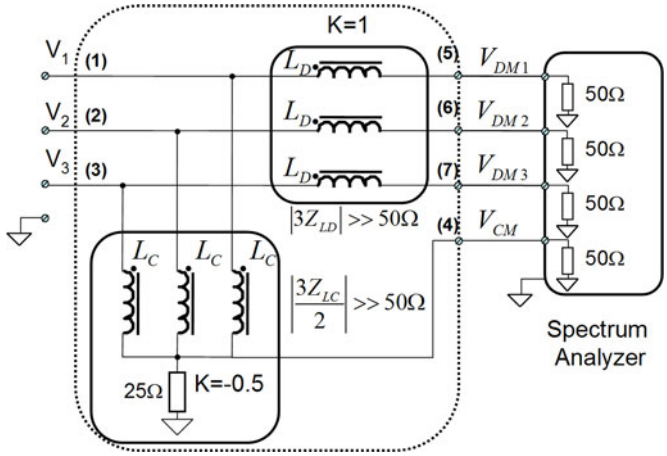

Fig. 12. Three-phase noise separator circuit.

other $n-1$ windings belonging to the other $n-1$ phases on the $n-1$ inductors, as shown in Fig. 11(a). Since the $n(n-1)/2$ inductors are identical, the coupling coefficient between any two L_Cs is $-1/(n-1)$. For two-phase noise separator [2] in single-phase power electronics systems, there is only one inductor with two coupled windings. Fig. 11(b) shows an example for a three-phase CM separation unit. The same cores used in the DM separation unit are used here for the inductor design. Each inductor has a 33-turn bifilar winding structure. The measured impedances of three inductors are almost the same. $|3Z_{LC}/2|$ is around 5.3 kΩ at 150 kHz, which is much larger than 50 Ω. The measured coupling coefficient between two windings is approximately -0.99999, so the leakage inductance is very small, and the coupling coefficient between two L_Cs is very close to $-1/2$. The inductors, therefore, meet the conditions defined previously.

The circuit and the prototype integrated with both DM and CM separation units are shown in Fig. 12. The port numbers are shown in the figure. Because the circuits of DM and CM separation units are different, the DM separation unit was built with a trifilar winding; on the other hand, the CM separation unit was built with bifilar windings as shown in Fig. 11(b).

V. Experimental Results

For an n-phase noise separator, there are n input ports and $n+1$ output ports; so there are total $2n+1$ ports. For the three-phase prototype in Fig. 12, there are total seven ports. Experiments are carried out for the three-phase prototype. The measured S-parameter is a 7×7 matrix. To evaluate the noise separator using (25), (31), (39)–(42), the measured S-parameters must be regrouped. The prototype is first evaluated with measured S-parameters and then used in a practical three-phase power electronics system for noise measurement.

A. Evaluation of the Developed Noise Separator

The S matrix for the developed three-phase noise separator is shown in (47). The S-parameters for the CM, DM1 (phase 1 DM noise), DM2 (phase 2 DM noise), and DM3 (phase 3 DM noise) separation functions are regrouped from (48) to (51):

TABLE I
Input Impedance of Port 1 With Different Source Impedances

	Z_S		300kHz-10MHz	10MHz-30MHz
Z_{in1}	0Ω	Magnitude	50Ω — 52.7Ω	50Ω — 55Ω
		Phase	-2° — 0.4°	-2° — -20°
	50Ω	Magnitude	50Ω — 51.2Ω	50Ω — 51.2Ω
		Phase	-1° — 0.4°	-1° — -7°
	∞Ω	Magnitude	50Ω — 50.6Ω	45Ω — 50Ω
		Phase	-0.2° — 0.4°	-0.2° — 10°

$$[S]=\begin{pmatrix} S_{11} & S_{12} & S_{13} & S_{14} & S_{15} & S_{16} & S_{17} \\ S_{21} & S_{22} & S_{23} & S_{24} & S_{25} & S_{26} & S_{27} \\ S_{31} & S_{32} & S_{33} & S_{34} & S_{35} & S_{36} & S_{37} \\ S_{41} & S_{42} & S_{43} & S_{44} & S_{45} & S_{46} & S_{47} \\ S_{51} & S_{52} & S_{53} & S_{54} & S_{55} & S_{56} & S_{57} \\ S_{61} & S_{62} & S_{63} & S_{64} & S_{65} & S_{66} & S_{67} \\ S_{71} & S_{72} & S_{73} & S_{74} & S_{75} & S_{76} & S_{77} \end{pmatrix} \quad (47)$$

CM separation S matrix

$$[S]=\begin{pmatrix} S_{11} & S_{12} & S_{13} & S_{14} \\ S_{21} & S_{22} & S_{23} & S_{24} \\ S_{31} & S_{32} & S_{33} & S_{34} \\ S_{41} & S_{42} & S_{43} & S_{44} \end{pmatrix} \quad (48)$$

DM1 separation S matrix:

$$[S]=\begin{pmatrix} S_{11} & S_{12} & S_{13} & S_{15(14)} \\ S_{21} & S_{22} & S_{23} & S_{25(24)} \\ S_{31} & S_{32} & S_{33} & S_{35(34)} \\ S_{51(41)} & S_{52(42)} & S_{53(43)} & S_{55(44)} \end{pmatrix} \quad (49)$$

DM2 separation S matrix:

$$[S]=\begin{pmatrix} S_{11} & S_{12} & S_{13} & S_{16(14)} \\ S_{21} & S_{22} & S_{23} & S_{26(24)} \\ S_{31} & S_{32} & S_{33} & S_{36(34)} \\ S_{61(41)} & S_{62(42)} & S_{63(43)} & S_{66(44)} \end{pmatrix} \quad (50)$$

DM3 separation S matrix:

$$[S]=\begin{pmatrix} \mathrm{S}_{11} & \mathrm{S}_{12} & \mathrm{S}_{13} & \mathrm{S}_{17(14)} \\ \mathrm{S}_{21} & \mathrm{S}_{22} & \mathrm{S}_{23} & \mathrm{S}_{27(24)} \\ \mathrm{S}_{31} & \mathrm{S}_{32} & \mathrm{S}_{33} & \mathrm{S}_{37(34)} \\ \mathrm{S}_{71(41)} & \mathrm{S}_{72(42)} & \mathrm{S}_{73(43)} & \mathrm{S}_{77(44)} \end{pmatrix}. \quad (51)$$

In order to directly use (25), (31), and (39)–(42) to evaluate the noise separator, the elements on the fourth row and the fourth column in (49), (50), and (51) need to be renumbered based on their row and column indices as shown in parentheses. Due to the frequency range limitation of the network analyzer (Agilent E5070B) used in the experiments, the S-parameters are measured from 300 kHz to 30 MHz. Input impedances, CMTR, CMRR_p, DMTR_p^m, and DMRR^m, are derived using (25), (31), and (39)–(42) and their values are shown in Tables I–III.

Table I shows the magnitude and phase for the input impedance of port 1 with different noise source impedances connected to the other two input ports. It is shown that the input impedance is very close to real 50 Ω, and it almost independent from the noise source impedance within the measured frequency range. Since the data of the other two input impedances

TABLE II
CMTR, DMRR[1], AND DMRR[2] WITH DIFFERENT SOURCE IMPEDANCES

	Z_S	300kHz-10MHz	10MHz-30MHz
CMTR	0Ω	0 — -0.55dB	-0.55dB—-1.2dB
	50Ω	0 — -0.55dB	-0.55dB—-1.7dB
	∞Ω	0 — -0.55dB	-0.55dB— -2dB
DMRR[1]	0Ω	<-46dB	<-40dB
	50Ω	<-46dB	<-40dB
	∞Ω	<-46dB	<-40dB
DMRR[2]	0Ω	<-46dB	<-40dB
	50Ω	<-46dB	<-40dB
	∞Ω	<-46dB	<-40dB

TABLE III
$DMTR_1^1$, $DMTR_1^2$, AND $CMRR_1$ WITH DIFFERENT SOURCE IMPEDANCES

	Z_S		300kHz-10MHz	10MHz-30MHz
$DMTR_1{}^1$	0Ω	Magnitude	0dB — -0.4dB	-0.4dB — -1.3dB
		Phase	0° — -17°	-17° — -42°
	50Ω	Magnitude	0dB — -0.3dB	-0.3dB — -0.8dB
		Phase	0° — -17°	-17° — -48°
	∞Ω	Magnitude	0dB — -0.2dB	-0.2dB — -0.3dB
		Phase	0° — -17°	-17° — -56°
$DMTR_1{}^2$	0Ω	Magnitude	0dB — -0.4dB	-0.4dB — -1.2dB
		Phase	0°— -16°	-17°— -41°
	50Ω	Magnitude	0dB— -0.3dB	-0.3dB — -0.8dB
		Phase	0°— -17°	-17°— -47°
	∞Ω	Magnitude	0dB — -0.2dB	-0.2dB — -0.2dB
		Phase	0°— -17°	-17° — -55°
$CMRR_1$	0Ω	Magnitude	<-40dB	<-34dB
	50Ω	Magnitude	<-40dB	<-34dB
	∞Ω	Magnitude	<-40dB	<-34dB

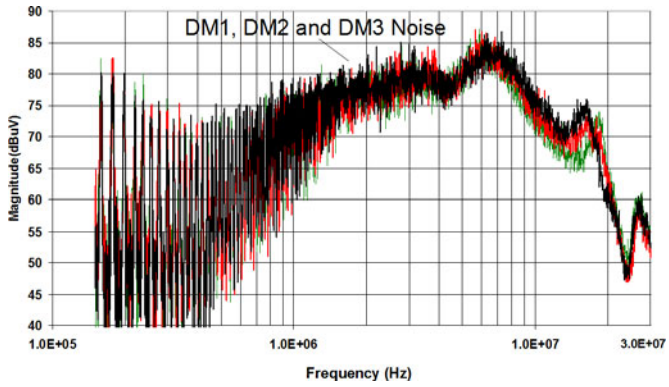

Fig. 13. Measured three-phase DM noise using the developed three-phase noise separator.

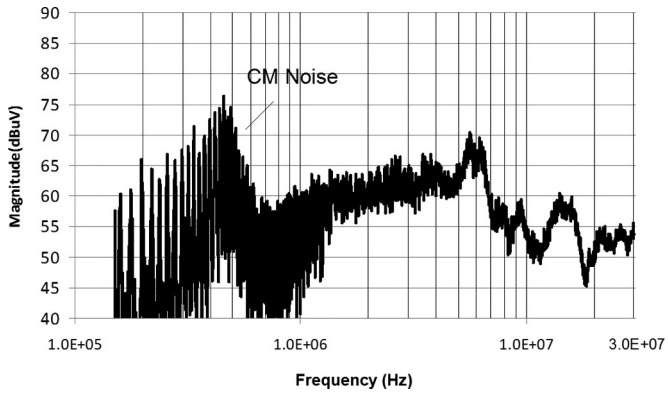

Fig. 14. Measured three-phase CM noise using the developed three-phase noise separator.

(not shown here) are very similar to the one shown in Table I, all the inputs of the noise separator can provide 50 Ω resistive input impedances, and they are independent from noise source impedances.

Table II shows the CMTR, $DMRR^1$, and $DMRR^2$ of the CM separation of the noise separator with difference noise source impedances. CMTR is very close to ideal 0 dB. The phase is not shown here since it is not important for CMTR. The calculated data show that $DMRR^1$ and $DMRR^2$ are independent from the noise source impedances. As analyzed earlier, $DMRR^1$ and $DMRR^2$ should be as small as possible. In Table II, both of them are smaller than −40 dB, so they are pretty good.

Table III shows the magnitude and phase of the $DMTR_1^1$, $DMTR_1^2$, and $CMRR_1$ of the DM1 noise separation unit with different noise source impedances. The $DMTR_2^1$, $DMTR_2^2$, and $DMTR_3^1$, $DMTR_3^2$ of the DM2 and DM3 noise separation units are almost the same as those of DM1 noise separation unit, so they are not shown here. Both $DMTR_1^1$ and $DMTR_1^2$ are very close to 0 dB. The calculated data also show that $DMTR_1^1$ and $DMTR_1^2$ have almost the same phase angle. As a result, the first and the second sequence noises at each frequency can be combined into DM noise at the output of the noise separator without any changes. The $CMRR_2$ and $CMRR_3$ of the DM2 and DM3 noise separation units are almost the same as $CMRR_1$ of DM1 noise separation unit, so they are not shown here. The CMRR should be as small as possible. $CMRR_1$ is smaller than −34 dB within the measured frequency range, so it is good.

B. EMI Noise Measurement Using the Developed Noise Separator

The noise separator was used to measure the DM and CM noises in a practical measurement setup, same as in Fig. 2. EUT is a 100-W three-phase ac/dc IGBT rectifier. If the noise is very high, three precision attenuators may be needed between the noise separator and LISNs to prevent the saturation of the cores. The output of the noise separator is connected to an Agilent E7402 A EMC analyzer. The unconnected outputs of the noise separator are terminated by 50 Ω terminators. The CM and DM peak noises are measured from 150 kHz to 30 MHz with a resolution bandwidth of 9 kHz. The measurement results are shown in Figs. 13 and 14.

Figs. 13 and 14 show that DM noise is dominant from 150 kHz to 4 MHz, and from 5 MHz to 22 MHz. From 4 MHz to 5 MHz and from 22 MHz to 30 MHz, CM noise is comparable with DM noise. Based on the measured DM and CM noises and the correspondent EMI standards, DM and CM EMI filters can be designed separately to meet the EMI standards with an appropriate margin. As a result, the sum or the difference of the DM and CM noises measured on LISNs meets the standards. This process guarantees that there is no overdesign, so it is more

efficient to achieve higher power densities and lower cost than the design process without the help of noise separators.

VI. Conclusion

In this paper, the EMI noise in a multiphase power electronics system is first analyzed using symmetrical component theory and EMI theory. The functions and critical parameters of multiphase noise separators are defined and modeled using symmetrical theory, S-parameter theory, and EMI theory. A circuit structure is proposed for multiphase noise separators. Design techniques for high-quality multiphase noise separators are explored. A multiphase noise separator prototype is developed, tested, and evaluated using the developed theory. The prototype is finally used in a practical power electronics system for EMI measurement.

References

[1] Y. Y. Maillet, R. Lai, S. Wang, F. Wang, R. Burgos, and D. Boroyevich, "High-density EMI filter design for DC-fed motor drives," *IEEE Trans. Power Electron.*, vol. 25, no. 5, pp. 1163–1172, May 2010.

[2] S. Wang, F. Lee, and W. G. Odendaal, "Characterization, evaluation, and design of noise separator for conducted EMI noise diagnosis," *IEEE Trans. Power Electron.*, vol. 20, no. 4, pp. 974–982, Jul. 2005.

[3] D. Zhang, D. Y. Chen, and D. Sable, "A new method to characterize EMI filters,," in *Proc. IEEE Appl. Power Electron. Conf. Expo.*, Anaheim, CA, Feb. 15–19,1998, pp. 929–933.

[4] R. Anderson, "Test and Measurement Application Note 95-1 S-Parameters Techniques," Hewlett-Packard, 1997.

[5] D. M. Pozar, *Microwave Engineering*. Hoboken, NJ: Wiley, 1998.

[6] N. Balabanian and T. Bickart, *Linear Network Theory: Analysis, Properties, Design, and Synthesis*. Beaverton, OR: Matrix, 1981.

[7] W. Medley, *Microwave and RF Circuits: Analysis, Synthesis, and Design*. Norwood, MA: Artech House, 1993.

[8] *Agilent AN154 S-Parameters Design Application Note*, Agilent Technol., 2000.

[9] P. S. Chen and Y. S. Lai, "Effective EMI filter design method for three-phase inverter based upon software noise separation," *IEEE Trans. Power Electron.*, vol. 25, no. 11, pp. 2797–2806, Jul. 2010.

[10] C. R. Paul and K. B. Hardin, "Diagnosis and reduction of conducted noise emissions," *IEEE Trans. Electromagn. Compat.*, vol. 30, no. 4, pp. 553–560, Nov. 1988.

[11] H.-L. Su and K.-H. Lin, "Computer-aided design of power line filters with a low cost common and differential-mode noise diagnostic circuit," in *Proc. IEEE Int. Symp. Electromagn. Compat.*, Montreal, Canada, Aug. 13–17, 2001, pp. 511–516.

[12] M. C. Caponet, F. Profumo, L. Ferraris, A. Bertoz, and D. Marzella, "Common and differential mode noise separation: Comparison of two different approaches," in *Proc. IEEE Power Electron. Spec. Conf.*, Vancouver, Canada, Jun. 17–21, 2001, pp. 1383–1388.

[13] M. C. Caponet and F. Profumo, "Devices for the separation of the common and differential mode noise: Design and realization," in *Proc. IEEE Appl. Power Electron. Conf. Expo.*, Dallas, TX, Mar. 10–14, 2002, pp. 100–105.

[14] M. L. Heldwein, J. Biela, H. Ertl, T. Nussbaumer, and J. W. Kolar, "Novel three-phase CM/DM conducted emission separator," *IEEE Trans. Ind. Electron*, vol. 56, no. 9, pp. 3693–3703, Sep. 2009.

[15] M. J. Nave, "A novel differential mode rejection network for conducted emissions diagnostics," in *Proc. IEEE Electromagn. Compat. Nat. Symp.*, Denver, CO, May 23–25, 1989, pp. 223–227.

[16] G. Ting, D. Y. Chen, and F. C. Lee, "Separation of the common-mode and differential-mode conducted EMI noise," *IEEE Trans. Power Electron.*, vol. 11, no. 3, pp. 480–488, May 1996.

[17] S. K. Yak and N. C. Sum, "Diagnosis of conducted interference with discrimination network," in *Proc. IEEE Power Electron. Drive Syst. Int. Conf.,* Singapore, Feb. 21–24, 1995, pp. 433–437.

[18] Y.-K. Lo, H.-J. Chiu, and T.-H. Song, "A software-based CM and DM measurement system for the conducted EMI," *IEEE Trans. Ind. Electron.*, vol. 47, no. 4, pp. 977–978, Aug. 2000.

[19] C. L. Fortescue, "Method of symmetrical coordinates applied to the solution of polyphase network," in *Proc. 34th Annu. Convention Amer. Inst. Electr. Eng.*, Atlantic City, NJ, Jun. 28, 1918, pp. 1027–1140.

[20] I. P. Macfarlane, "A probe for measurement of electrical unbalance of networks and devices," *IEEE Trans. Electromagn. Compat.*, vol. 41, no. 1, pp. 3–14, Feb 1999.

[21] A. Nagel and R. W. De Donker, "Separating common mode and differential mode noise in EMI measurements," in *Proc. EPE Conf.*, Lousanne, 1999, pp. 1–8.

[22] J. Sevick, *Transmission Line Transformers*. Newington, CT: American Radio Relay League, 1987.

Shuo Wang (S'03–M'06–SM'07) received the Ph.D. degree from the Center for Power Electronics Systems (CPES), Virginia Tech, Blacksburg, in 2005.

From 2005 to 2009, he was with CPES, Virginia Tech. From 2009 to 2010, he was with the Electrical Power Systems Group, GE Aviation Systems, Vandalia, OH. Since 2010, he has been with the Department of Electrical and Computer Engineering, University of Texas at San Antonio, San Antonio. He is the holder of five U.S. patents and has two others pending. He has published more than 80 journal and conference papers. His research interests include electromagnetic interference/electromagnetic compatibility in power electronics systems, high-density power conversion, three-phase power conversion and inversion, motor drives, generator control, power systems, and microgrid.

Dr. Wang is an Associate Editor for the IEEE Transactions on Industry Applications and a lead Guest Editor for a special issue of online journal, *Advances in Power Electronics*. He was the recipient of the 2005 Best Transactions Paper Award from the IEEE Transactions on Power Electronics and the William M. Portnoy Award at the IEEE Industry Applications Society Annual Conference in 2004.